Optimization of Single-Walled Carbon Nanotube Arrays for Methane Storage at Room Temperature

Dapeng Cao,*,†,‡,§ Xianren Zhang,† Jianfeng Chen,† Wenchuan Wang,† and Jimmy Yun‡

Research Center of Ministry of Education for High Gravity Engineering and Technology, College of Chemical Engineering, Beijing University of Chemical Technology, Beijing 100029, China, and NanoMaterials Technology Pte Ltd, 26 Ayer Rajah Crescent #07-02, Singapore 139944, Singapore

Received: July 18, 2003; In Final Form: September 24, 2003

The adsorption storage of methane on triangular arrays of single-walled carbon nanotubes (SWNT) at room temperature was investigated by the grand canonical Monte Carlo (GCMC) method. In the simulation, carbon atoms on the tubular wall were structured according to the (*m*, *m*) armchair arrangement, and the site-to-site method was used to calculate the interaction between a methane molecule inside the tube and a carbon atom on the tubular wall. Excess volumetric and gravimetric endohedral adsorptions of methane in the (15,15), (20, 20), (25, 25), and (30, 30) SWNT arrays were obtained. For every armchair SWNT array above, the van der Waals (VDW) gap has been varied from 0.335 to 1.0 nm to optimize methane storage in the interstices of SWNT arrays. The usable capacity ratio (UCR), which is defined as the mass of available fuel in an adsorbent-loaded vessel divided by the mass of available fuel in a vessel without adsorbent, was used as the criterion to judge the adsorption performance of SWNT arrays with different parameters. Results indicate that the (15, 15) SWNT arrays with a VDW gap of $\Delta = 0.8$ nm is the optimal adsorbent among all of the cases studied for methane storage at room temperature. At $p = 4.1$ M Pa, the total volumetric and gravimetric capacities (including endohedral and exohedral adsorption) of methane on the SWNT arrays with the optimal parameters reach 216 V/V and 215 g CH_4/kg C, respectively. It not only greatly exceeds the target (150 V/V) of the Department of Energy (U.S.A.) but also is slightly greater than the capacity (200 V/V) of compressed natural gas at 20 M Pa. The attainment of the exciting result attributes to the optimization of the VDW gap parameter of SWNT arrays, because the adsorption of methane in the interstices surpasses 60% of the total amount at the optimal condition, while its value is less than 15% of the total amount at a VDW gap of $\Delta = 0.335$ and $p = 4.1$ M Pa.

1. Introduction

With the development and progress of human society, the fossil fuels of coal, petroleum, and others are consumed drastically. Exploiting new and effective alternative energy sources is urgently required. In addition, emission control calls for using clean fuels for vehicles. Accordingly, hydrogen and natural gas, in which methane is the main component, are commonly considered to be suitable alternatives without pollution. Therefore, how to efficiently store natural gas has become an important subject. Compared to compressed natural gas (CNG) technology, adsorption natural gas (ANG) technology[1] is very promising and efficient, because ANG requires a relatively low pressure of about 4 M Pa to be stored in a lightweight carrier, whereas CNG is often stored in heavy steel cylinders at high pressures, 20∼30 M Pa.

In past years, a lot of investigations about methane adsorption storage on different porous materials (including molecular sieves,[2−7] layered pillared pore materials,[8,9] activated carbon,[10−27] carbon nanotubes,[28−43] etc.) were published. Tan and Gubbins[10] studied the adsorption of methane in a slit carbon pore at supercritical temperatures and pointed out that the classical excess adsorption isotherms from molecular simulation exhibit a maximum adsorption at a specific pressure, as expected by experimental measurements. Du et al.[2] investigated the adsorption of methane in zeolites by using mean-field theory and Monte Carlo (MC) simulation. Zhou[12] used the experimental method to measure the adsorption of methane at supercritical temperatures, and they obtained a storage capacity of 176 g CH_4/kg C at $T = 293$ K. Lozano-Castello et al.[17] used different binders of powdered activated carbon to study methane storage and found that one optimum binder makes the capacity reach 192 k CH_4/kg C at room temperature 298 K. In another paper by them,[18] the volumetric capacity of 165 V/V of methane on activated carbon was also reported. Miyawaki and Kaneko [19] investigated the adsorption storage of methane in activated carbon fibers, and obtained a maximum gravimetric capacity of 140 g CH_4/kg C at room temperature. Herbst and Harting[20] obtained a maximum gravimetric capacity of 145 g CH_4/kg C at room temperature by experimentally measuring the adsorption of methane on activated carbon Norit R1. Although their goals that the storage capacity of methane exceeds the target of the Department of Energy (DOE, U.S.A),[18] 150 V/V (i.e., 150 STP liters of gas stored per liter vessel volume), were basically reached, their results fall short of the capacity (200 V/V) of CNG at 20 M Pa.[16] Extensive experimental and theoretical works have also been reviewed by Menon et al.[26] and Lozano-Castello et al.[27] The details are available in their references, so we do not intend to discuss these works further here.

* To whom correspondence should be addressed. E-mail: cao_dp@hotmail.com

† Beijing University of Chemical Technology.

‡ NanoMaterials Technology Pte Ltd.

§ Present address: Department of Chemical and Environmental Engineering, University of California, Riverside, CA 92521.

10.1021/jp036094r CCC: $25.00
Published on Web 11/08/2003

Since the carbon nanotube was first discovered by Iijima in 1991,[28] there have been many published studies on the application of carbon nanotubes, especially the application of single-walled carbon nanotube (SWNT).[29−41] Of which most paid the attention on hydrogen storage on SWNTs or SWNT arrays,[30−36] because hydrogen is the cleanest fuel that can achieve zero emission through fuel cells. However, a long time is needed to make the commercial application of hydrogen come true. Therefore, adsorption storage of methane on a SWNT or SWNT array should also be paid some attention.[37−41] Most recently, Bekyarova et al.[42] studied the adsorption of methane in a single wall nanohorn (SWNH) by experimental measurement, and the measured volumetric capacity reached 160 V/V. Kaneko and co-workers[38] used a density functional theory (DFT) method to study the adsorption of methane on isolated SWNT and found that the excess gravimetric capacity reached 198 g CH_4/kg C at room temperature and 4.0 M Pa when the reduced pore size of SWNT is 4.2.

As seen from the statement above, the isolated SWNT is an excellent candidate for methane storage at room temperature. Unfortunately, to our knowledge, there are few reports[39−41] available for the adsorption storage of methane on SWNT arrays. Muris et al. [39] only studied the adsorption and phase behavior of methane on SWNTs at low temperatures. Talapatra et al.[40] experimentally measured the adsorption of CH_4, Ne, and Xe on SWNT bundles and unexpectedly observed that no gases adsorbed on the interstices of SWNT arrays, which only indicates that it is the sample of SWNT bundles used in their experiment that cannot adsorb gases. However, it dose not mean that the interstice of other SWNT arrays cannot adsorb gas. Sequentially, in another paper from them,[41] they observed that methane can adsorb on the bundles of closed-end SWNT.

As a result, the aim of this research work is to investigate the adsorption storage of methane on SWNT arrays by using the grand canonical Monte Carlo (GCMC) method. According to the observation of our previous study on hydrogen storage on SWNT arrays,[36] the van der Waals (VDW) gap is a primary factor that affects the adsorption amount of methane in the interstices of SWNT arrays. Therefore, we focused our attention on the optimization of the VDW gap between tubes in SWNT arrays to obtain a maximal capacity of methane storage.

2. Potential Models and Simulation Details

2.1. Potential Models. In this work, as in the works of many researchers, the cut and shifted Lennard-Jones (LJ) potential was used to represent the interaction between methane molecules[10,13]

$$\phi_{ff}(r) = \begin{cases} \phi_{lj}(r) - \phi_{lj}(r_c) & r < r_c \\ 0 & r \geq r_c \end{cases} \quad (1)$$

where r is the interparticle distance, r_c is the cutoff radius, $r_c = 5\sigma_{ff}$. ϕ_{lj} is the full LJ potential, $\phi_{LJ}(r) = 4\epsilon_{ff}[(\sigma_{ff}/r)^{12} - (\sigma_{ff}/r)^6]$, where ϵ_{ff} and σ_{ff} are the energy and size parameters of the fluid. They are 148.1 and 0.381 nm for methane here, respectively.

The interaction between the wall and a methane molecule inside a tube of SWNT arrays is calculated by the site-to-site method[9]

$$\phi_{in} = 4\epsilon_{fw} \sum_{i=1}^{N_f} \sum_{j=1}^{N_{carbon}} \left[\left(\frac{\sigma_{fw}}{r_{ij}} \right)^{12} - \left(\frac{\sigma_{fw}}{r_{ij}} \right)^{6} \right] \quad (2)$$

where N_f is the number of methane fluid molecules, N_{carbon} is the number of carbon atoms of the wall of SWNT. ϵ_{fw} and σ_{fw} are the cross-energy and size parameters, which are obtained from the Lorentz−Berthelot (LB) combining rules. Energy and size parameters of carbon atom are 28.0 and 0.34 nm, respectively. r_{ij} is the distance between a fluid methane molecule and an atom of the wall of SWNT. In this work, the SWNT was arranged according to the (m, m) armchair.[29] For the (m, n) SWNT, the diameter and the chiral angle are respectively

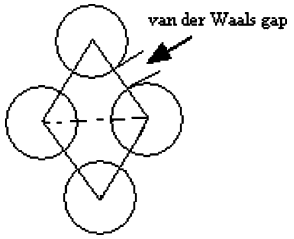

Figure 1. Cross section of the triangular array of SWNT.

$$D = b/\pi \sqrt{3(m^2 + mn + n^2)}$$

and

$$\theta = \tan^{-1}[-\sqrt{3}n/(2m + n)]$$

where $b = 0.142$ nm is the C−C bond length.

For the methane in the interstices of SWNT arrays, the adsorbate−adsorbent interaction potential is obtained by integration of the LJ potential over the outer surface of the nanotube and is given by[43]

$$\phi_{out}(r, R) = \pi^2 \epsilon_{fw} \rho_{surf} R \sigma_{fw}^2 r^{-1} \left[\frac{63}{32} \left[\frac{r^2 - R^2}{\sigma r} \right]^{-10} F\left[-9/2, -9/2; 1; \left(1 - \frac{r}{R}\right)^2 \right] - 3 \left[\frac{r^2 - R^2}{\sigma r} \right]^{-4} F\left[-3/2, -3/2; 1; \left(1 - \frac{r}{R}\right)^2 \right] \right] \quad (3)$$

where $F[\alpha,\beta;\gamma;\chi]$ is the hypergeometric series, R is the radius of a tube, and r is the distance from the wall, $\rho_{surf} = 38.2$ nm^{-2} is the density of carbon atoms on the wall.[36,38]

2.2. Simulation Details. Using the grand canonical Monte Carlo (GCMC) method, where the temperature, the chemical potential, and the pore volume are the independent variables and are specified in advance, the adsorptions of methane inside SWNT and in the interstices between SWNTs at room temperature were simulated. SWNT bundles were arranged in a triangular array, as shown in Figure 1. A unit cell contains one tube and two interstices.[33] For adsorption of methane inside SWNT, the periodic boundary condition was imposed only in the axis direction (z direction),[3] whereas for adsorption of methane in interstices between SWNTs, the periodic boundary conditions were employed in all directions.[34] The relationship between the chemical potential and the bulk pressure was solved by the MBWR equation of Johnson et al.[44] for the LJ fluid, because the chemical potential and temperature of methane in confinement spaces are equal to those of the bulk phase in the adsorption equilibrium. An initial configuration was generated randomly before the GCMC simulation. In the simulation, all variables were reduced with respect to the methane parameters.

In addition, for every state, 2×10^7 configurations were generated. The former 1×10^7 configurations were discarded to guarantee equilibration, whereas the latter 1×10^7 configurations were used to average the desired thermodynamic proper-

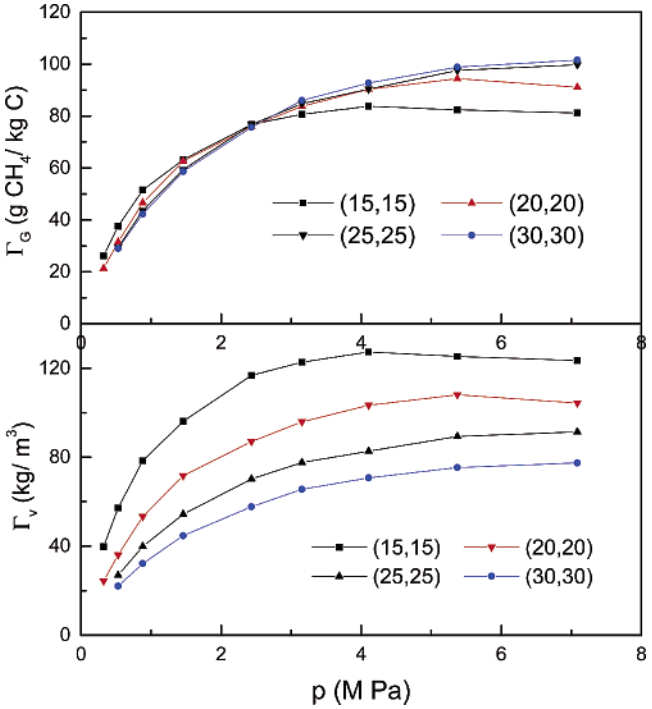

Figure 2. Endohedral excess adsorption of methane in SWNT arrays.

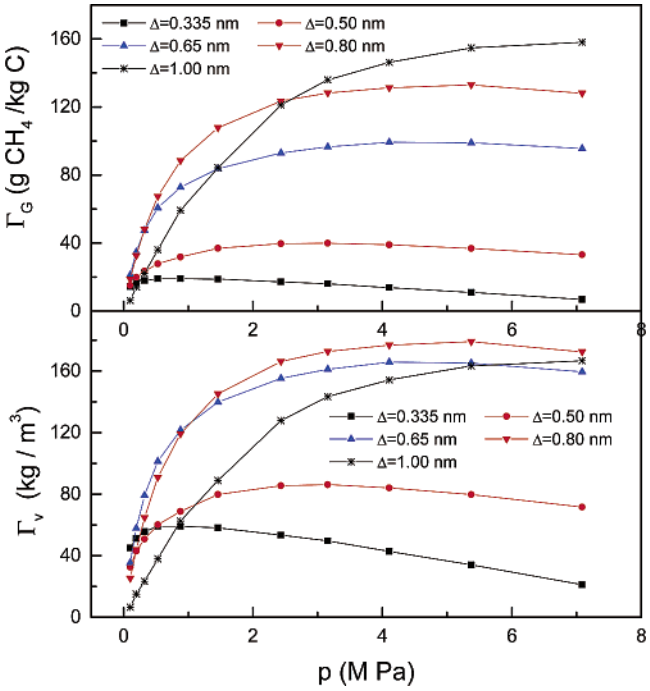

Figure 3. Excess adsorption of methane in the interstice of the (15, 15) SWNT array.

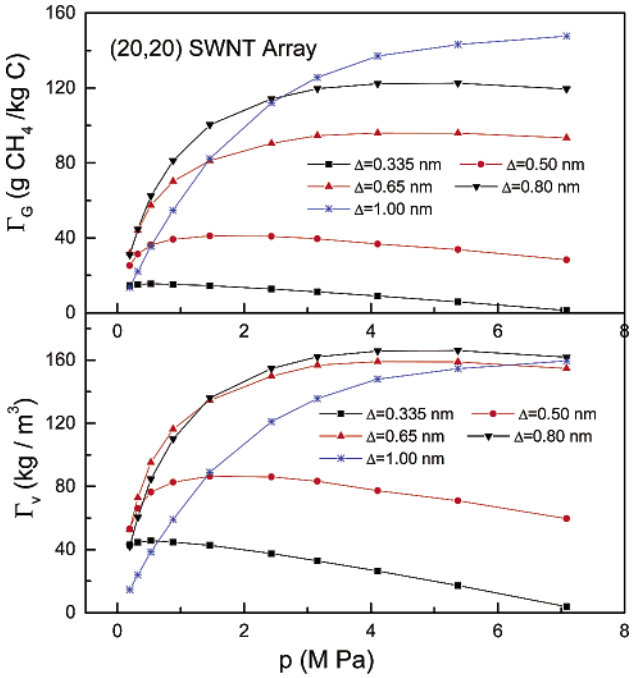

Figure 4. Excess adsorption of methane in the interstice of the (20, 20) SWNT array.

ties. The uncertainty on the final results (ensemble averages of the number of adsorbate molecules in the box and the total potential energy) is estimated to be less than 2%. Other simulation details can be referred to in our previous work.[9]

3. Results and Discussion

Adsorption storages of methane in intratubular and interstitial channels of SWNT arrays were simulated. In the work, all simulations were carried out at room temperature $T = 300$ K. The following commonly used variables are calculated

Excess volumetric adsorption, Γ_v

$$\Gamma_v = \frac{m_{CH_4} - m^0_{CH_4}}{V} \tag{4}$$

Excess gravimetric adsorption, Γ_G

$$\Gamma_G = \frac{m_{CH_4} - m^0_{CH_4}}{m_{SWNT}} \tag{5}$$

where m_{CH_4} is the total mass of methane presented in the calculated volume, m_{SWNT} is the total mass of SWNT, $m^0_{CH_4}$ is the mass of methane in the bulk phase, and V is the calculated volume. For the adsorption of methane inside the tube, V represents the intratubular volume. For the adsorption of methane in the interstice, V represents the interstitial volume. For the total adsorption of methane on SWNT arrays, V represents total volume of the unit cell studied.

3.1. Adsorption of Methane inside SWNT Arrays. We have simulated the adsorption isotherms of methane inside SWNT with four different diameters. They are 2.03, 2.71, 3.39, and 4.07 nm, corresponding to the (15,15), (20,20), (25,25), and (30, 30) armchair arrangements, respectively. Endohedral adsorption isotherms represented by excess volumetric and excess gravimetric capacities were shown in Figure 2. One can see that, at the low-pressure range $P < 3.1$ M Pa, the excess gravimetric capacities almost keep the same for the four diameter SWNTs studied, whereas at the pressure range of $P > 3.1$ M Pa, the larger diameter SWNT has the higher excess gravimetric capacity. However, the excess volumetric capacity decreases with the increase in pore size of SWNT. This is because the gradient of the increase in mass of adsorbed methane is smaller than the gradient of the increase in intratubular volume when the diameter of SWNT increases.

3.2 Adsorption of Methane in the Interstices of SWNT Arrays. Figures 3−6 show the excess gravimetric and excess volumetric adsorption isotherms of methane in the interstices of SWNT arrays with different van der Waals gaps. In our work, five van der Waals gaps ($\Delta = 0.335$, 0.5, 0.65, 0.8, and 1.0

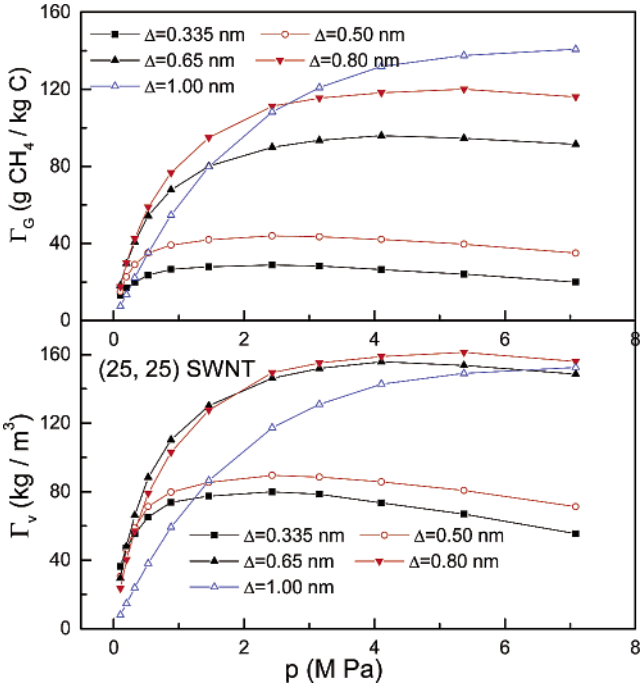

Figure 5. Excess adsorption of methane in the interstice of the (25, 25) SWNT array.

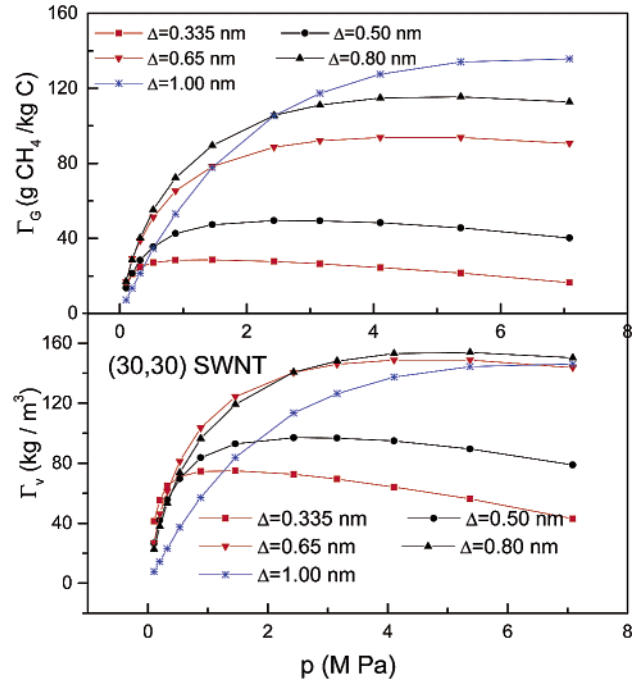

Figure 6. Excess adsorption of methane in the interstice of the (30, 30) SWNT array.

nm) were used. It can be observed from Figure 3 that, among all VDW gaps studied, the SWNT array with a 0.335 nm VDW gap shows the smallest excess gravimetric and excess volumetric capacities, where Γ_G of methane is less than 20 g CH_4/kg C and Γ_v of methane is less than 50 kg /m^3. Moreover, they decrease and trend to zero when the pressure increases to 7.1 M Pa. This is because the interstice with $\Delta = 0.335$ nm has the most space unaccessible for methane molecules, which results in the adsorbed methane molecules almost being the same as the bulk phase at high-pressure $P = 7.1$ M Pa. The finding can provide a possible explanation for the result from Talapatra et al. [40] that methane cannot adsorb in the interstice of SWNT bundles. It is because the VDW gap of SWNT bundles employed in their experiment must be 0.335 nm, which leads to almost no gases absorbed on the interstices. At $\Delta < 0.8$ nm, Γ_G of methane increases with the increase of the VDW gap. However, at $\Delta = 1.0$ nm, Γ_G of methane is smaller than that of $\Delta = 0.8$ nm at the low-pressure range of $P < 2.4$ M Pa, although the SWNT array with a 1.0 nm VDW gap displays the highest Γ_G at the high-pressure range of $P > 2.4$ M Pa. It is a main reason that, at a VDW gap of $\Delta = 1.0$ nm, the decreasing interaction potential causes the reduction of adsorption amount of methane at the low-pressure range of $P < 2.4$ M Pa. However, at the high-pressure range of $P > 2.4$ M Pa, high-pressure forces more molecules into the adsorbed phase, which leads to the SWNT array with a 1.0 nm VDW gap holding higher uptake than that of the 0.8 nm VDW gap. For Γ_v, it is the SWNT array with $\Delta = 0.8$ nm, rather than the $\Delta = 1.0$ nm SWNT array, that holds highest uptake at the whole pressure range studied.

For the (20, 20), (25, 25), and (30, 30) SWNT arrays, the Γ_v and Γ_G of methane in interstices present the same behavior as that of the (15, 15) SWNT array when the VDW gap changed from 0.335 to 1.0 nm. They can be clearly observed in Figure 4−6, respectively.

3.3. Optimization of the VDW Gap. According to the analysis above, it is difficult to determine the optimal VDW gap. Seen from the Γ_v, the 0.8 nm VDW gap is a optimal gap, whereas observed from Γ_G, the 1.0 nm VDW gap is a optimal gap at $P > 2.4$ M Pa.

The excess volumetric and gravimetric storage capacities are not the only measures of adsorption. In addition, our target is to obtain more usable methane gas. Accordingly, the usable capacity ratio (UCR),[34] which is an important criterion used to judge the performance of an adsorbent, can meet our requirement. It is a measure of the effectiveness of physisorption compared with gas compression at the same pressure. The UCR is defined as the mass of available fuel in an adsorbent-loaded vessel divided by the mass of available fuel in a vessel without adsorbent (compressed gas only). The available fuel, in the case methane, is defined as[34]

$$\Gamma_{fuel} = \Gamma_{ads} - \Gamma_{dis} \tag{6}$$

where Γ_{ads} is the mass of methane in the vessel at the storage pressure, and Γ_{dis} is the mass of methane in the vessel at the discharge pressure. In this work, the 1.01 atm was chosen as the discharge pressure.

Generally, the medium-pressure range of 3∼6 M Pa was often considered as the adsorption pressure. So we focused our attention on the following four pressures, 2.43, 3.15, 4.11, and 5.37 M Pa. Figure 7 shows the UCRs changing with the VDW gap for different SWNT arrays at the four fixed pressures. It can be observed from the (15, 15) SWNT array that, at $P =$ 2.43 M Pa, the UCR increases from 1.4 to 9.6 when the VDW gap increases from 0.335 to 0.8 nm. The UCR reaches its highest value at $\Delta = 0.8$ nm. Interestingly, it is not only the (15, 15) SWNT array but also the (20, 20), (25, 25), and (30, 30) SWNT arrays that exhibit the same behavior that UCR reaches its largest value at $\Delta = 0.8$ nm. Surprisingly, it is a great coincidence that the Γ_v also reaches its highest uptake at $\Delta = 0.8$ nm. As a result, $\Delta = 0.8$ nm was considered to be the optimal VDW gap for methane storage.

After the optimal VDW gap $\Delta = 0.8$ nm was determined, the pore size of SWNT should be taken into account. Here the total excess adsorptions (including excess volumetric and gravimetric adsorption) were used for our aim at determination of pore size of the tube. For the total excess gravimetric

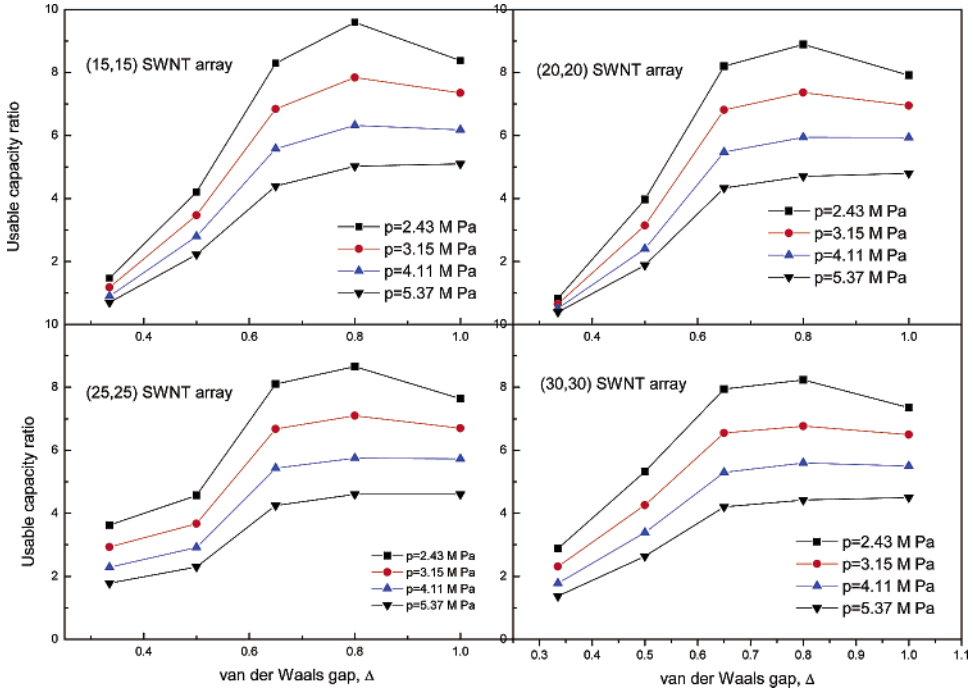

Figure 7. UCR changing with VDW gap for different SWNT arrays at four pressures.

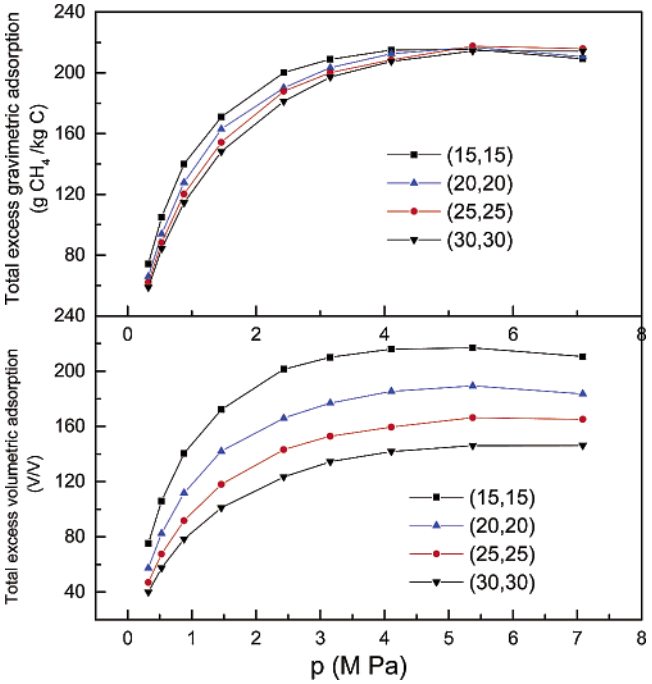

Figure 8. Total excess adsorption of methane in SWNT arrays.

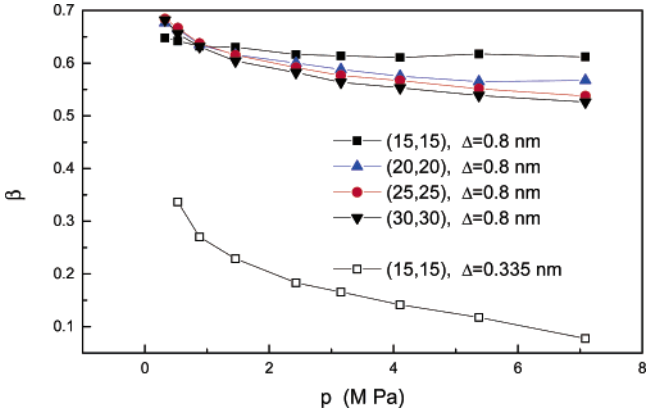

Figure 9. Ratio of the excess adsorption of methane in the interstice to the total excess amount.

adsorption, it is a simple sum of excess adsorption of methane inside tube and excess adsorption of methane in interstices with $\Delta = 0.8$ nm. However, the total excess volumetric adsorption cannot use the simple sum like gravimetric adsorption, because volumetric adsorption is an intensive variable. It should be defined as the total excess mass of methane in the investigated unit cell (including one tube and two interstices) divided by the total volume of the unit cell. Figure 8 shows the total excess adsorptions of methane in different size SWNT arrays. Note that the V/V unit was used to describe the total excess volumetric adsorption in Figure 8, for a direct comparison with an experimentally measured volumetric capacity. The total excess volumetric and excess gravimetric adsorptions both indicate that the (15, 15) SWNT array has the highest uptake at $p = 4.1$ M Pa. The UCR also exhibit an excellent agreement with it. Namely, the (15,15) SWNT array displays the highest UCR compared to those of the other three diameter SWNT arrays in the same conditions. Accordingly, the (15, 15) SWNT array with $\Delta = 0.8$ nm was considered to be the optimal candidate of the adsorbents for methane storage.

For emphasizing the importance of optimization of SWNT arrays, we also calculated the ratio (β) of excess adsorption of methane in the interstice to total excess adsorption, and the ratio was shown in Figure 9. It can be clearly seen that, at the optimal VDW gap, the excess adsorption of methane in the interstice is larger than 52% of total excess adsorption for all pore size SWNT arrays. Especially for the (15, 15) SWNT array, the excess adsorption of methane in the interstice exceeds 60% of the total amount. However, at a VDW gap of $\Delta = 0.335$ nm, the ratio is less than 15% at $P = 4.1$ M Pa. Moreover, with the increase in pressure, the ratio continuingly decreases down to zero. Apparently, the optimization of the VDW gap of SWNT arrays significantly improves the methane storage capacity.

It is noticeable that 0.8 nm is not a clear-cut optimum, because it is rather difficult to achieve this value in the manufacture of SWNTs. In addition, if the array arrangement is different from

TABLE 1: Comparisons of Our Results and the Experimentally Measured Data

sources	materials	Γ_G (g CH_4/kg C)	volumetric capacity (v/v)	temp (K)	pressure (M Pa)
Herbst et al. [20]	activated carbon, Norit R1	144		298	0.95
Inomata et al. [22]	activated carbon pellet		164	298	3.5
Lozano et al. [18]	powered activated carbon	168	165	298	4.0
Lozano et al. [7]	carbon molecular sieve	192		298	4.0
Chen et al. [6]	meso-carbon microbead		185	298	5.0
Zhou L et al. [12]	activated carbon	176		293	6.0
Zhou L et al. [16]	wet activated carbon		200	273	10.0
Quinn et al. [21]	activated carbon monoliths		180	298	6.9
Bekyarova et al. [42]	single wall carbon nanohorn		160	303	3.5
Miyawaki et al. [19]	activated carbon fiber P20	140		300	6.3
Tanaka et al. [38]	isolated SWNT (DFT)	198		303	4.05
this work	(15,15)SWNT array, $\Delta = 0.8$	215	216	300	4.11

triangle, the optimum spacing of 0.8 would vary accordingly. However, our calculation provides a good approach for advising manufactures of carbon nanotubes.

3.4. Comparison of Our Results and the Experimentally Measured Data. The results of methane storage on SWNT arrays at the optimal condition in this work and the experimentally measured data for methane storage on different carbon materials were compared and listed in Table 1.

Obviously, the volumetric and gravimetric capacities of methane in this work both greatly exceed the listed data from different carbon materials. As mentioned previously, although the listed data all surpass the DOE target, they fall short of the CNG capacity (200 V/V) at 20 M Pa. Only the result of Zhou et al.[16] is close to the CNG capacity at the expense of high pressure ($P = 10.0$ M Pa). Interestingly, the simulated volumetric capacity (216 V/V) at the optimal parameter condition slightly exceeds the CNG capacity. Simultaneously, the simulated gravimetric capacity also reaches 215 g CH_4/kg C. Our investigation indicates that the potential of SWNT arrays for methane storage is superior to that of activated carbon, which is a good agreement with the result from Yin et al. [35] about hydrogen storage. The finding above is theoretically positive evidence for the practical operation application of methane storage on the SWNT arrays at room temperature.

4. Conclusions

The adsorption storage of methane on triangular arrays of SWNT at room temperature was investigated by the GCMC method. In the simulation, carbon atoms on the tubular wall were structured according to the (*m*, *m*) armchair arrangement, and the site-to-site method was used to calculate the interaction between a methane molecule inside the tube and a carbon atom on the tubular wall. The (15,15), (20, 20), (25, 25), and (30, 30) SWNT arrays with VDW gaps that were varied from 0.335 to 1.0 nm were used as the adsorbents for methane storage. For the adsorption of methane in the interstices of SWNT arrays, the VDW gap plays a primary role in the storage capacity. A usable capacity ratio was used as the criterion to judge the adsorption performance of SWNT arrays on optimizing the VDW gap to gain maximal methane uptake. Results indicate that the (15, 15) SWNT arrays with a VDW gap of $\Delta = 0.8$ nm is the optimal adsorbent among all of the cases studied for methane storage at room temperature. At $P = 4.1$ M Pa, the total volumetric and gravimetric capacities (including endohedral and exohedral adsorption) of methane on the (15, 15) SWNT arrays with $\Delta = 0.8$ nm reach 216 V/V and 215 g CH_4/kg of C, respectively. It not only exceeds the DOE target but also is slightly greater than the CNG capacity (200 V/V) at 20 M Pa. The attainment of the exciting result is attributable to the optimization of parameters of SWNT arrays, because the adsorption of methane in the interstices surpasses 60% of the total amount at the optimal condition, whereas its value is less than 15% of the total amount at $P = 4.1$ M Pa and VDW gap $\Delta = 0.335$. In short, our investigation indicates that SWNT arrays are excellent candidates for methane storage.

Acknowledgment. This work was supported by the Key Research of Science & Technology of the Ministry of Education, China (No. 0202), the National Key Fundamental Research Plan of China (No. G2000048010), and Innovation Development Scheme (IDS) by Economic Development Board of Singapore.

References and Notes

(1) Matranga, K. R.; Myers, A. L.; Glandt, E. D. *Chem. Eng. Sci.* **1992**, *47*, 1569.
(2) Du, Z. M.; Dunne, L. J.; Chaplin, M. F.; Manos, G. *Chem. Phys. Lett.* **1999**, *307*, 413.
(3) Cao, D. P.; Chen, J.; Shen, Z.; Zhang, X.; Wang, W. *Acta Chim. Sinica* **2002**, *60*, 820.
(4) Yun, J. H.; Duren, T.; Keil, F. J.; Seaton, N. A. *Langmuir* **2002**, *18*, 2693.
(5) Clarkson, C. R.; Bustin, R. M.; Levy, J. H. *Carbon* **1997**, *35*, 1689.
(6) Chen, X. S.; McEnaney, B.; Mays, T. J.; Alcaniz-Monge, J.; Cazorla-Amoros, D.; Linares-Solano, A. *Carbon* **1997**, *35*, 1251.
(7) Lozano-Castello, D.; Cazorla-Amoros, D.; Linares-Solano, A.; Quinn, D. F. *J. Phys. Chem. B* **2002**, *106*, 9372.
(8) Cao, D. P.; Wang, W. C. *J. Colloid Interface Sci.* **2002**, *254*, 1; *Acta Chim. Sin.* **2001**, *59*, 297.
(9) Cao, D. P.; Wang, W. C. *Phys. Chem. Chem. Phys.* **2001**, *3*, 3150; **2002**, *4*, 3720.
(10) Tan, Z.; Gubbins, K. E. *J. Phys. Chem.* **1990**, *94*, 6061.
(11) Jiang, S.; Rhykerd, C. L.; Gubbins, K. E. *Mol. Phys.* **1993**, *79*, 273.
(12) Zhou, L.; Zhou, Y.; Li, M.; Chen, P.; Wang, Y. *Langmuir* **2000**, *16*, 5955.
(13) Cao, D. P.; Wang, W. C.; Shen, Z.; Chen, J. *Carbon* **2002**, *40*, 2359.
(14) Cao, D. P.; Wang, W. C. *Chem. J. Chin. Univ.* **2002**, *23*, 910.
(15) Gusev, V. Y.; OBrien, J. A.; Seaton, N. A. *Langmuir* **1997**, *13*, 2815.
(16) Zhou, L.; Sun, Y.; Zhou, Y. P. *AIChE J.* **2002**, *48*, 2412.
(17) Lozano-Castello, D.; Cazorla-Amoros, D.; Linares-Solana, A.; Quinn, D. F. *Carbon*, **2002**, *40*, 2817; *Carbon* **2002**, *40*, 989.
(18) Lozano-Castello, D.; Cazorla-Amoros, D.; Linares-Solano, A. *Energy Fuels* **2002**, *16*, 1321.
(19) Miyawaki, J.; Kaneko, K. *Chem. Phys. Lett.* **2001**, *337*, 243.
(20) Herbst, A.; Harting, P. *Adsorption* **2002**, *8*, 111.
(21) Quinn, D. F.; Ragan, S. *Adsorp. Sci. Technol.* **2000**, *18*, 515.
(22) Inomata, K.; Kanazawa, K.; Urabe, Y.; Hosono, H.; Araki, T. *Carbon* **2002**, *40*, 87.
(23) Nguyen, T. X.; Bhatia, S. K.; Nicholson, D. *J. Chem. Phys.* **2002**, *117*, 10827.
(24) Biloe, S.; Goetz, V.; Guillot, A. *Carbon* **2002**, *40*, 1295.
(25) Alcaniz-Monge, J.; Dela-Casalillo, M. A.; Cazorla-Amoros, D.; et al. *Carbon* **1997**, *35*, 291.
(26) Menon, V. C.; Komarneni, S. *J. Porous Mater.* **1998**, *5*, 43.
(27) Lozano-Castello, D.; Alcaniz-Monge, J.; de la Casa-Lillo, M. A.; Cazorla-Amoros, D.; Linares-Solano, A. *Fuel* **2002**, *81*, 1777.
(28) Iijima, S. *Nature*, **1991**, *354*, 56; *Physica B* **2002**, *323*, 1.

(29) Lin, M. F.; Shyu, F. L. *Phys. Lett. A* **1999**, *259*, 158.
(30) Liu, C.; Fan, Y. Y.; Liu, M.; Cong, H. T.; Cheng, H. M.; Dresselhaus, M. S. *Science* **1999**, *286*, 1127.
(31) Dillon, A. C.; Jones, K. M.; Bekkedahl, T. A.; Kiang, C. H.; Bethune, D. S.; Heben, M. J. *Nature* **1997**, *386*, 377.
(32) Chen, P.; Wu, X.; Lin, J.; Tan, K. L. *Science* **1999**, *285*, 91.
(33) Wang, Q.; Johnson, J. K. *J. Chem. Phys.* **1999**, *110*, 577.
(34) Wang, Q.; Johnson, J. K. *J. Phys. Chem. B* **1999**, *103*, 4809.
(35) Yin, Y. F.; Mays, T.; McEnaney, B. *Langmuir* **2000**, *16*, 10521.
(36) Zhang, X. R.; Cao, D. P.; Chen, J. F. *J. Phys. Chem. B* **2003**, *107*, 4942.
(37) Zhang, X. R.; Wang, W. C. *Fluid Phase Equilib.* **2002**, *194*, 289.
(38) Tanaka, H.; El-Merraoui, M.; Steele, W. A.; Kaneko, K. *Chem. Phys. Lett.* **2002**, *352*, 334.
(39) Muris, M.; Dufau, N.; Bienfait, M.; Dupont-Pavlovsky, N.; Grillet, Y.; Palmari, J. P. *Langmuir* **2000**, *16*, 7019.
(40) Talapatra, S.; Zambano, A. Z.; Weber, S. E.; Migone, A. D. *Phys. Rev. Lett.* **2000**, *85*, 138.
(41) Talapatra, S.; Migone, A. D. *Phys. Rev. B* **2002**, *65*, 045416.
(42) Bekyarova, E.; Murata, K.; Yudasaka, M.; Kasuya, D.; Iijima, S.; Tanaka, H.; Kahoh, H.; Kaneko, K. *J. Phys. Chem. B* **2003**, *107*, 4681.
(43) Gordon, P. A.; Saeger, R. *Ind. Eng. Chem. Res.* **1999**, *38*, 4647.
(44) Johnson, J. K.; Zollweg, J. A.; Gubbins, K. E. *Mol. Phys.* **1993**, *78*, 591.